LABORATORY OF NUCLEAR MEDICINE AND RADIATION BIOLOGY

900 VETERAN AVENUE

UNIVERSITY OF CALIFORNIA, LOS ANGELES, CALIFORNIA 90024

AND DEPARTMENT OF RADIOLOGY

UCLA SCHOOL OF MEDICINE, LOS ANGELES, CALIFORNIA 90024

These studies were supported by Contract #DE-AM03-76-SF00012 between the U.S. Department of Energy and the University of California

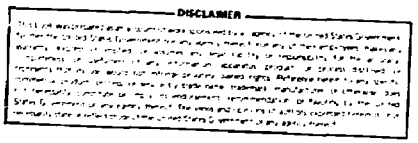

Prepared for the U.S. Department of Energy under Contract #DE-AM03-76-SF00012

CEREBRAL EXTRACTION OF N-13 AMMONIA: ITS DEPENDENCE ON CEREBRAL BLOOD FLOW AND CAPILLARY PERMEABILITY - SURFACE AREA PRODUCT

Michael E. Phelps, Ph.D., Sung Cheng Huang, D.Sc., David E. Kuhl, M.D., Edward J. Hoffman, Ph.D., and C. Slin, M.S.

ABSTRACT

^{13}N-labeled ammonia was used to investigate i) the cerebral extraction and clearance of ammonia, ii) the mechanism by which capillaries accomodate changes in cerebral blood flow CBF and iii) its use for the measure of CBF. This was investigated by measuring the single pass extraction of $^{13}NH_3$ in rhesus monkeys during P_aCO_2 induced changes in CBFand with dog studies using in vitro tissue counting techniques to examine $^{13}NH_3$ extraction in gray and white matter, mixed tissue and cerebellum during variations in CBF produced by combinations of embolization, local brain compression, and changes in P_aCO_2. The single pass extraction fraction of $^{13}NH_3$ varied from about 70 to 20% over a CBF range of 12 to 140cc/min/100gms. Capillary permeability-surface area product (PS) estimates from this data and the dog experiments with a Renkin/Crone model show PS increasing with CBF. The magnitude and rate of increase in PS with CBF was highest in gray matter > mixed tissue > white matter. Tissue extraction of $^{13}NH_3$ vs CBF relationship was best described by a unidirectional transport model in which CBF increases by both recruitment of capillaries and by increases of blood velocity in open capillaries. This saturable-recruitment model provides a possible explanation for the mechanism of flow changes at the capillary level. Glutamine synthetase, which incorporates $^{13}NH_3$ into glutamine appears to be anatomically located in astrocytes in general and specifically in the astrocytic pericapillary end-feet that are in direct contact with gray and white matter capillaries (Norenberg, M.D., Martinez-Hernandez, A. (1979) Brain Res. 151:303-310). The net $^{13}NH_3$ extraction subsequent to an i.v. injection increases nonlinearly with CBF. Doubling or halving basal CBF produced from 40 to 50% changes in the ^{13}N tissue concentrations with further increases in CBF associated with progressively smaller changes in ^{13}N concentrations. $^{13}NH_3$ appears to be a good tracer for the detection of cerebral ischemia with positron tomography but exhibits a poor response at high values of CBF.

INTRODUCTION

(N-13) ammonia ($^{13}NH_3$)* has been used as an imaging agent for the heart and brain since it was originally proposed by Hunter et al (11,21) and Harper et al (8), with very little information regarding what factors determine its tissue distribution. The rapid diffusion of $^{13}NH_3$ through cerebral (26,30) and myocardial (37) capillaries and its rapid incorporation and trapping in the slowly turning over amino acid pools can potentially allow the use of this labeled substrate for imaging capillary perfusion, the study of the capillary flow mechanisms or the study of ammonia and amino acid metabolism. However, due to the complexities involved in the extraction and retention of $^{13}NH_3$ in these organs, more extensive studies are required to better understand the potential uses of this tracer.

Phelps et al (26) using positron computed tomography (PCT) with normal volunteers, have shown high uptake of $^{13}NH_3$ in cortex of the cerebrium, internal gray nuclei and cerebellum relative to white matter with relative ^{13}N concentrations in good agreement with the relative capillary densities and/or cerebral blood flow (CBF). Subsequently, Phelps, et al (30) used a single pass extraction technique in the monkey to demonstrate that the single pass extraction of $^{13}NH_3$ by the brain was i) less than 100% in the CBF range of 20 to 100 cc/min/100 gm, ii) inversely related to CBF, iii) not affected by blood ammonia concentrations from 80 to 1400 µg% or by changes in arterial blood pH over the range 7.2 to 7.7, iv) decreased by about 40% when the cerebral metabolic rate for glucose and oxygen was reduced by factor of 2.5 by inducing a hypoglycemic coma and v) not affected when blood ammonia concentration was increased by a factor of 6 during hypoglycemia even though the cerebral metabolic rate for glucose increased by a factor of 2.2. We also found that $^{13}NH_3$ extraction was limited by

capillary permeability and reported a value for the permeability coefficient of $^{13}NH_3$ in brain (30). Intravenously injected $^{13}NH_3$ was also proposed as a tracer for the estimate of capillary perfusion in brain and heart in analogy to the microsphere model with capillary occlusion by microspheres replaced by metabolic trapping of $^{13}NH_3$ (26,30).

Carter et al (4) and more recently Lockwood et al (19) evaluated the effect of blood pH and ammonia concentration on $^{13}NH_3$ uptake in brain. Lockwood et al (19) using $^{13}NH_3$ to investigate ammonia metabolism in patients with liver disease and hyperammonemia, proposed a model for the measurement of the brain utilization rate of ammonia with $^{13}NH_3$.

Cooper et al (5) also studied the effect of ammonia concentration, measured ammonia turnover rates and determined the metabolic fate of exogenous $^{13}NH_3$ by chemical assay methods. They observed rapid ammonia metabolism that occurs primarily via the reaction of glutamate with ammonia at a half time of 1 to 3 sec or less (5) and was anatomically located in the astrocytes. This has been experimentally verified by Norenberg and Martinez-Hernandez (22) using an ultrastructural immunocytochemical technique to determine the distribution of the glutamine synthetase in the rat brain. They found glutamine synthetase almost exclusively confined to astrocytes with equal concentrations in astrocytes of gray and white matter and the highest concentration in the astrocytic pericapillary end-feet.

We have investigated the relationship of net cerebral extraction and the single pass extraction fraction of $^{13}NH_3$ as a function of CBF in order to examine the rate limiting steps and mechanisms in the cerebral extraction of $^{13}NH_3$. An intracarotid bolus injection-single pass extraction method was used to measure extraction fractions of $^{13}NH_3$ as a function of P_aCO_2 induced CBF changes in monkeys. A dog model employing in vitro tissue sampling, local brain

compression, distributed embolitic infarction and/or variations in P_aCO_2 was used to measure net cerebral extraction of $^{13}NH_3$ as a function of CBF. In this model, local tissue values of ^{13}N tissue concentrations for gray matter, white matter, cerebellum and mixed gray/white matter were determined by surgical dissection of the brain.

The tissue uptake and clearance and the equilibrium distribution of ^{13}N in the brain of man after i.v. injection of $^{13}NH_3$ was measured with PCT and compared to the distribution of cerebral metabolic rate for glucose with FDG. The dependence of $^{13}NH_3$ extraction on the cerebral capillary permeability-surface area product (PS) and the rapid metabolic trapping of $^{13}NH_3$ in astrocytes provides a means of accurately estimating the PS of different cerebral structures. The relationship between PS and CBF was estimated in terms of a number of unidirectional transport models and a saturable-recruitment model is proposed to describe the mechanism for CBF changes at the capillary level. The use of $^{13}NH_3$ and other non-flow limited tracers for the measure of capillary blood flow was examined.

MATERIALS AND METHODS

Preparation of $^{13}NH_3$

$^{13}NH_3$ was produced with the UCLA medical cyclotron as described elsewhere (40). $^{13}NH_3$ was buffered to pH 7.4 in physiologic saline prior to injection. The radiochemical purity was greater than 99% and ammonia concentration was less than 10^{-4} M.

Animal Preparation

Twentytwo, 20 to 30 kgm, mongrel dogs were anesthetized with sodium pentobarbital (25 mg/kgm), paralyzed with gallamine triethiodide and ventilated

on room air or mixtures of CO_2 and O_2. A polyethylene cannula in the left atrium was used for injection of labeled microspheres and/or $^{13}NH_3$. Systemic blood pressure was monitored with a catheter in the aorta connected to a staatham pressure transducer. This catheter was also used for withdrawal of arterial blood samples. End tidal PCO_2 was continuously monitored with a Beckman LB50 capnograph.

In five dogs, the left common carotid artery was isolated for injection of 30mg of 100-200 micron diam. resin to embolize portions of the brain. Two were also ventilated with 5% CO_2 - 95% O_2 and three with 10% CO_2 - 90% O_2. Arterial blood gases, pH and ammonia concentrations were determined by standard clinical laboratory techiques.

In twelve dogs a small inflatable ballon was inserted into the subdural space through a burr hole on one side of the calvarium to produce local compressions of the brain. Five were ventilated with 5% CO_2 - 95% O_2 and seven were ventilated on room air. In five other dogs, two were ventilated on room air and three were ventilated with 10% CO_2 - 90% O_2 with no other intervention performed.

Seven rhesus monkeys were anesthetized with pentobarbital sodium (5 mg/kgm) 2 to 4 weeks prior to experimentation and the right external carotid artery ligated at its origin. At the time of the experiment, the animals were again anesthetized and a 0.2 mm diam. catheter positioned in the right common carotid artery. The animals were paralyzed with gallamine triethiodide and passively ventilated on room air or different CO_2 - O_2 admixtures (5, 7 or 10% CO_2) and anticoagulated with heparin. The arterial catheter was used for injection of $^{13}NH_3$ and ^{133}Xe, monitoring of arterial blood pressure and sampling of blood for P_aCO_2, pH, ammonia analysis.

Measurement of CBF, $^{13}NH_3$ Extraction Fraction and Net $^{13}NH_3$ Extraction

Global CBF: Global CBF was measured in the rhesus monkeys by the 10-min

height/area method (45) from the clearance curve resulting from a 0.2 cc bolus internal carotid artery injection of ^{133}Xe (30). The final value of CBF was calculated assuming the ^{133}Xe 10-min height/area method systemically overestimates flow by 11% (9) and using a whole brain partition coefficient for Xe of 1.10 ml/gm (41).

Local CBF: The local CBF in the in vitro dog studies was determined by the quantitative microsphere technique (12). Carbonized polystyrene microspheres of 15 ± 5 microns were suspended in 10% dextran with one drop of tween 80 to prevent clumping, thoroughly mixed with a vortex shaker and suspended by ultrasonification just prior to injection. Approximately $2x10^5$ microspheres labeled with ^{125}I, ^{141}Ce, or ^{85}Sr were injected into the left atrium. Just prior to injection of microspheres and $^{13}NH_3$, arterial blood withdrawal was initiated at a constant rate and continued for 2.5 minutes. The total microsphere radioactivity in this sample and the microsphere radioactivity from excised samples of known weight were measured in a well counter. The local CBF was then calculated by;

$$CBF\ (cc/min/100gms) = (F_p \times C_i \times 100)/C_b \qquad (1)$$

Where F_p is the pump withdrawal rate of arterial blood (cc/min), C_i is the microsphere tissue radioactivity concentration in region i (counts/min/gm) and C_b is the total microsphere activity in arterial blood sample (counts/min).

Extraction Fraction: The fraction (E) of $^{13}NH_3$ extracted by the brain during a single capillary transit was determined by extrapolation of the tail of the washout curve, which is the extracted and retained $^{13}NH_3$ in the tissue, back to the initial peak of the curve, which is the total $^{13}NH_3$ activity input to the tissue. E is then estimated from the ratio of the extrapolated value to the peak value (30,25).

Net Extraction The net tissue extraction (i.e. ^{13}N tissue concentration) of

$^{13}NH_3$ in the in vitro dog experiments was determined in the same manner as the CBF in eq. 1. The input function (i.e. C_b for ^{13}N in eq.1) corresponded to only ^{13}N in the form of $^{13}NH_3$ by correcting for the contribution due to metabolized ^{13}N (Schelbert et al, unpublished work: 90% of ^{13}N activity is free $^{13}NH_3$ from time of injection to 2.5 min.)

Animal Procedures

Single Pass Measure of E vs CBF: In the single pass measurements of E, the monkey was stabilized at a basal P_aCO_2, a 0.2cc bolus of ^{133}Xe injected into the internal carotid and data collected for 11 min for the measurement of CBF. A 0.2 cc bolus of $^{13}NH_3$ dissolved in the animals plasma was then injected into the internal carotid and data collected for the next 20 to 30 min. The P_aCO_2 level was then increased or decreased by varying the inhaled CO_2 concentration and/or respiratory rate. Fifteen minutes was allowed for equilibration at each P_aCO_2 level before ^{133}Xe and $^{13}NH_3$ were injected. End tidal CO_2 was monitored to assure constant P_aCO_2 levels. Arterial blood samples were taken before and after each injection for blood gas and pH measurement.

Local net extraction of $^{13}NH_3$ vs CBF: In the in vitro dog experiments, variations in local CBF were produced by embolism, variation in P_aCO_2, and local compression. Five dogs were subjected to embolization followed by 15 min of 5% CO_2 - 95% O_2 or 10% CO_2 - 90% O_2 to produce a wide range of local CBF. Microspheres and $^{13}NH_3$ were simultaneously injected into the left atrium for the measurement of CBF and net tissue $^{13}NH_3$ extraction. Arterial samples were taken prior to and after embolization, after 15 min blood gas equilibrium, and just prior to end of experiment for blood gas, pH and ammonia analysis.

After 5 min the animals were terminated by a rapid injection of high concentration KCL into the heart. The brain was rapidly excised, cut into transverse sections and twenty to thirty 0.3 to 1 gm samples taken from cortical

gray matter, white matter and cerebellum. The samples were immediately counted for ^{13}N activity, weighed (including the blood sample) decay corrected and the counts/time/weight determined. After the ^{13}N activity ($t_{1/2}$ - 10 min) had decayed, the samples were counted to determine the tissue concentration and total blood activity of microspheres.

Extreme care was taken to dissect out individual samples of cortical gray and white matter (cerebellum samples contained both gray and white matter). The samples were visually classified into gray, white and mixed gray-white matter. The short half life of ^{13}N required rapid dissections of the brain which limited our ability to obtain pure gray and white matter samples. The degree of admixture of the gray and white matter samples was estimated by their CBF ratio in each experiment.

The procedure was repeated for 2 dogs at basal P_aCO_2 and 3 dogs ventilated with 10% CO_2 - 90% O_2 without embolization and 6 dogs in which a local compression was produced by inflation of the balloon in the subdural space with the dog on 5% CO_2 - 95% O_2 or room air.

In three other dogs the above protocol was changed by adding the injection of labeled microspheres in the basal state, inflation of the subdural balloon and a second injection of microspheres (labeled with a different radionuclide from the first) and $^{13}NH_3$ five min after inflation of the balloon. Three additional dogs were studied in which microspheres were injected in the basal state, the balloon was inflated for 30 min, deflated and 30 minutes later $^{13}NH_3$ and a second set of labeled microspheres were injected. In this series of dog experiments tissue samples were taken without separation into gray and white matter.

Arterial blood clearance rates were determined by monitoring the activity with a femoral artery catheter which passed through a NaI well counter and to a withdrawal pump. The catheter had a total volume of 2.1 cc and blood was

withdrawn at a rate 4.29 cc/min. The data sampling time (initially 0.1 sec) and catheter produced only minor distortion of the blood clearance rate (tested with step impulse injected into the catheter).

Human Studies

Six male volunteers (age 21-26) were studied by tomographically measuring the distribution of ^{13}N in the brain after an i.v. bolus injection of 10 to 15 mCi of $^{13}NH_3$. Tomographic scans with the ECAT† positron tomograph (28) were started 4 to 5 min after injection with initial scan times of 2 to 3 min and the time progressively increased in proportion to ^{13}N decay rate. From 4 to 8 scans were made per injection and contained from 700,000 to 1.5 million counts per image. Data are automatically decay corrected and photon attenuation corrected with a geometric method (26,28) before images were reconstructed. The concentration ratio between different substructures of the brain were measured as previously described (28) and compared to the distribution of the local cerebral metabolic rate for glucose as measured with (F-18)fluorodeoxyglucose, FDG (14,33,29,10).

Three male volunteers (age 21-23) were injected intravenously with $^{13}NH_3$ and images of a single cross-section of the brain imaged as a function of time. After injection, four 2 min scans, four 4 min scans and six 10 min scans were performed to cover a 90 minute period. Region of interest analysis was performed to measure the average and the gray and white matter tissue uptakes and clearance rates.

Unidirectional Transport Model

A starting point for the description of the cerebral extraction of $^{13}NH_3$ is the Renkin/Crone model for the unidirectional transport through a capillary membrane (34,6) as initially formulated by Kety (13). This model assumes: i) the capillary is a rigid tube, ii) exponential decrease in tracer blood concentrations along the capillary, iii) intravascular concentration of tracer is much larger than extravascular, iv) extravascular volume of distribution is infinitely larger than

intravascular, and v) the capillary membrane is the rate limiting step in the extraction or the tracer. This model is described by

$$E = 1-e^{-PS/F} \qquad (2)$$

or

$$\ln (1-E) = -PS/F \qquad (3)$$

Where E is the unidirectional extraction fraction for the tracer, P and S are the capillary permeability (cm/min) and surface area (cm^2/100gm) and F is the capillary blood flow (cc/min/100gm).

Strict application of this model to a multi-capillary environment would require that all the capillaries be identical in length and diameter (i.e. S), P and F. This assumption is not valid for global measurements of E in the brain. Since the relationship between E and PS is nonlinear, the sum of local values of E for the whole brain cannot be used to calculate the sum of local PS values from Eq. 2. It has been shown previously (34) that the PS from eq 2 underestimates the sum of PS values in heterogenous tissues. The result is an "effective" PS value which is an underestimation of the true value of the total PS (34). This model also assumes that the value of PS is constant as a function of flow (i.e. capillaries are rigid tubes) and that capillary flow increases by velocity and not by changes in the number of open capillaries (i.e. recruitment), vasodilitation or frequency of opening and closing of capillaries.

By changing these assumptions, various extended forms of the Renkin/Crone model can be derived to describe the relationship between E and F. For example, by assuming the tissue consists of various sizes of capillaries each with a different PS value but obeying the original Renkin/Crone assumptions, E will have the following functional form.

$$E = 1-(A_1 e^{-PS_1/F} + A_2 e^{-PS_2/F} + \ldots + A_i e^{-PS_i/F}) \qquad (4)$$

Where $\sum_i A_i = 1$. In this paper a model with two compartments was tested.

Alternatively, if capillary recruitment is included in the model (i.e. as flow is increased more capillaries become active) and all capillaries are identical and behave like rigid tubes, then E would have the same functional form as the Renkin/Crone Model (Eq. 2), except PS is not constant. Since PS will not increase indefinitey, a non divergent function for PS was examined in this paper. That is,

$$E = (1 - e^{-PS/F})$$

with (5)

$$PS = A + B(1 - e^{-CF})$$

We refer to this model as the saturable-recruitment (SR) model. At saturation (i.e. all capillaries are open and active) the sum of A and B will be equal to the PS of all the anatomical capillaries in a given type of tissue. The value of C indicates the rate at which any given tissue will approach saturation as flow increases. The extraction of $^{13}NH_3$ as a function of CBF was analyzed with each of the above forms (eqs. 2,4,5) to determine which provided the best fit to the data.

RESULTS

Human Studies

Figure 1 illustrates the cerebral distribution of $^{13}NH_3$ subsequent to an i.v. injection as compared to cerebral metabolic rate for glucose (CMRGlc) in normal human volunteers. The average ^{13}N tissue concentration ratio of gray (frontal, temporal, parietal, occipital and visual cortex) to white matter (frontal, parietal and occipital) was found to be 1.77 ± 0.18 (s.d.) as compared to 1.91 ± 0.23 for the CMRGlc in 6 normal volunteers (20 levels total with an average of twelve 0.7 to 1.4 cm^2 regions/level). These values are in good agreement with those of Kuhl et al (15) who found values of 1.69 ± 0.15 (s.d.) for ^{13}N and 1.88 ± 0.17 for CMRGlc in normal man.

Cerebral tissue ^{13}N concentration was found to rapidly reach a high level in two to three minutes, slowly increase for the next 50 min (~15% increase) and then slowly decrease with about a 2.3 hour half time (Fig. 2). There appeared to be some tendency for gray matter to clear ^{13}N at a faster rate, but the clearance rates of both tissues were so slow that the data did not demonstrate a significant difference. The time variation of the tissue ^{13}N concentration is consistent with the rapid blood clearance of $^{13}NH_3$ (5% and 1 to 2% of the peak value at 2 and 10 min after injection), its rapid diffusion into cerebral tissue and the slow turnover rate of the tissue ^{13}N activity.

Single Pass Studies

The whole brain single pass extraction fraction E from carotid bolus studies in monkeys in Figure 3, demonstrates that E decreases as CBF increases. However, net extraction of $^{13}NH_3$ (E times CBF) or tissue ^{13}N concentration increases nonlinearly with CBF (Fig. 5A). The increase in net extraction with CBF is due to the fact that the rate of increase in CBF (i.e. amount of $^{13}NH_3$ delivered to tissue) more than compensates for the decrease in E.

Figure 4 is a plot of the single pass E data assuming a Renkin/Crone model (eq 2). If a Renkin/Crone model were adequate to describe the data, one would have seen a linear relationship between ln(1-E) and 1/CBF with the slope equal to - PS. This is clearly not the case.

The average tissue clearance rate of the extracted portions of $^{13}NH_3$ subsequent to the intracarotid injection was found to be 1.4 ± 0.5 hours (s.d.).

Net Extraction Studies

The net extraction (i.e. tissue ^{13}N concentration and equivalent of E times CBF from single pass studies) vs. CBF for mixed gray-white matter and cerebellum (mixed gray/white matter) are shown in Figure 5B and 5C when local changes in CBF were produced by combinations of embolization, variations in

P_aCO_2 and local brain compressions. The plot of the net extraction vs CBF for mixed gray/white matter for animals subjected to only local compressions of the brain is shown in Figure 5D. Figure 5E and 5F show the net extractions for gray and white matter as a function of CBF that were measured when CBF changes were induced by alterations in P_aCO_2, embolization and local compressions. No apparent difference in the net extraction vs CBF was noted in these maneuvers to produce a wide range of local CBF values. To check the amount of admixture in samples classified as gray or white matter, we calculated the gray/white matter CBF ratio. The average value for the samples shown in Figures 5E and 5F and Table 1 was 2.31 ± 0.61, which is lower than the average value for ratio of CBF in gray to white matter of about 2 to 4 for anethezised animals (16,38,39). This indicated that samples were reasonably pure but did still contain significant gray/white matter admixtures as was also noted visually.

Figure 6 illustrates the local tissue variations from basal CBF (^{125}I microspheres) to the CBF values (^{141}Ce microspheres) and ^{13}N tissue concentrations during a local compression for both the involved and contralateral hemisphere. The increases and decreases in CBF are followed very closely by ^{13}N tissue concentrations except that response of the ^{13}N concentration is less than the actual CBF changes as would be expected from figure 5.

The equations from the least square fits to SR model (eq. 5) for the global single pass study, gray matter, white matter, mixed gray-white matter, cerebellum and compression are given in table 1. A combined plot of these equations are shown in figure 7 for comparison of the different experimental measurements. The data fits to the Renkin/Crone model (eqs. 2 & 3) and multicomponent (Eq. 4) models were considerably worse (i.e. significantly larger sum of squares) than the fit by SR model (eq. 5). The data in table 1 were also used to calculate the PS product as a function of CBF as shown in Figure 8.

DISCUSSION

N-13 ammonia is extracted exclusively from the capillaries due to their large surface to volume ratio and is then trapped in the tissue primarily by its rapid incorporation into glutamine as diagramed in Figure 9. Thus,the tissue ^{13}N distribution is specific to blood flow at the at the capillary level and is analogous to microsphere technique with capillary occlusion replaced by metabolic trapping. $^{13}NH_3$ deposition in tissue is not however strictly flow limited and primarily depends upon capillary perfusion, permeability-surface area product (PS) and the tissue ammonia pool turnover rate of the metabolic trapping process (26,30,5,25). These properties should enable $^{13}NH_3$ to be used to examine the mechanisms of capillary perfusion, to accurately measure PS for ammonia and possibly to use this tracer for the imaging of the distribution of CBF in man with positron tomography. This complexity requires one to carefully examine the factors which affect the extraction, trapping and clearance of $^{13}NH_3$ by the brain.

Mechanism for Extraction and Trapping of $^{13}NH_3$

The uncharged $^{13}NH_3$ is assumed to be the species transported into the tissue, as a result of its higher lipid solubility and the low permeability of the blood brain barrier (BBB) for charged molecules. With a pK_a of 9.02 (42), the charged NH_4^+ species predominates at normal blood pH values. However, the rate of exchange between the two species is so rapid (1.9×10^{-5} sec to establish equilibrium), that it is unlikely that this exchange is the rate limiting step and $^{13}NH_3$ that diffuses out of the plasma is continuously replenished from the interconversion with $^{13}NH_4^+$ (30).

The permeability of $^{13}NH_3$ through the BBB is probably largely determined by its limited lipid solubility (30). Raichle, et al (32) have shown an excellent correlation between lipid solubility and the BBB permeability of various alcohols

which is consistent with the lipid solubility dependance reported by Pappenheimer (24). This is also consistent with the fact that $^{13}NH_3$ is not 100% extracted by the brain at normal values of CBF.

It is well known that the ammonia pool in brain is small, about 0.2 mM (20). Cooper et al (5) using $^{13}NH_3$, a rapid freeze brain blowing technique and direct chemical assay methods have found the half time for the ammonia pool turnover to be 1 to 3 sec or less. Cooper et al (5) found that greater than 80% of the ^{13}N was in the amide group of glutamine after a 10 min carotid artery infusion of $^{13}NH_3$. The remainder of ^{13}N was accounted for with about 16% as free ammonia, 1% in the α-amino group of glutamine, 0.3% in glutamate and the remainder in various other amino acids. Their data clearly showed that rapid turnover of ammonia in brain was occuring by the reaction of ammonia with a small pool of glutamate and glutamine synthetase (5) as had been proposed earlier by Berl et al (1). The experiments of Cooper et al (5) eased some of the concern over the validity of the results of Berl et al (1) who used such large masses of $^{15}NH_3$ that brain ammonia concentrations were about 10 times normal values.

Cooper et al (5) proposed that glutamine synthetase was primarily located in astrocytes. Norenberg and Martinez-Hernandez (22) using a ultrastructural immunocytochemical technique have found glutamine synthetase to be almost exclusively located in astrocytes of the rat brain with the astrocytic pericapillary end-feet showing the highest concentration, high concentration in astroglial of the neuropil, equal concentration in cerebral cortex and striatum and generally that white and gray matter astrocytes had equal concentrations.

From the above and our previous work (26,30,25) it appears that under normal conditions i) the rate limiting step for extraction of $^{13}NH_3$ by brain is due to its limited BBB permeability ii) that the metabolic trapping occurs in the small glutamate-glutamine synthetase pool located in astrocytes, iii) the general large

distribution of astrocytes in brain and their specific proximity to capillaries (astrocytic pericapillary end-feet) provide an efficient mechanism for general trapping of $^{13}NH_3$ diffusing from both gray and white matter capillaries and iv) the net extraction of $^{13}NH_3$ depends primarily upon CBF, capillary PS product and integrity of the glutamate - glutamine synthetase reaction.

$^{13}NH_3$ Extraction vs CBF

Phelps et al (30) demonstrated from single pass extraction studies that the extraction fraction, E, of $^{13}NH_3$ was inversely related to CBF. These investigators reported a linear relationship between ln(1-E) vs 1/CBF (eq. 2) and used the Renkin/Crone model to estimate a value for whole brain PS product. Now with many more single pass studies (Fig. 3) it is clear that the relationship between ln(1-E) and 1/CBF is not linear (Fig. 5). This indicates that the simple Renkin/Crone model for capillaries cannot describe the CBF vs E relationship for $^{13}NH_3$ unless the PS product is allowed to increase as CBF increases (see later discussion).

Phelps et al (25) used a combination of intracarotid and intravenous injections of $^{13}NH_3$, and a vascular tracer to determine the unidirectional transport of $^{13}NH_3$ and assess the amount of back diffusion. It was concluded that the size of the extravascular space for $^{13}NH_3$ diffusion and the rapid incorporation of $^{13}NH_3$ into amino acides normally prevents significant back diffusion. We reexamined this by the same technique and arrived at the same conclusion. Thus E is assumed to be the unidirectional extraction fraction. Estimates of back diffusion at low CBF are most important since PS estimates are very sensitive to errors in E when the value of E is high. Also at low CBF, back diffusion is most difficult to resolve from the vascular and the trapped components of the curve.

Since local back diffusion cannot be determined from the dog studies

employing in vitro tissue counting in this work, we compared average values of E from the single pass carotid studies with the mixed gray/white matter tissue values from the in vitro tissue sampling studies (Figs 3,5, and Table 1). At CBF values of 20 and 40cc/min/100gms, single pass values of E were 0.57 ± 0.05 and 0.43 ± 0.05 and values from mixed gray/white matter in the dog studies were 0.54 ± 0.11 and 0.42 ± 0.05. Since these values are in good agreement, back diffusion was assumed to be the same for both techniques for mean CBF values of ≥ 20cc/min/100gm. The rapid blood clearance of i.v. injected $^{13}NH_3$ probably accounts for this fact (41,34). Cooper et al (5) found that constant $^{13}NH_3$ levels in blood for 10 min in the rat allowed back diffusion and equilibration of the intra- and extravascular compartments which in turn led to reduced values of E.

At the extremely low values of local CBF produced by embolization and compression, ^{13}N tissue concentrations were disproportionately higher than the microsphere tissue concentrations. This may be due to high extraction of $^{13}NH_3$ at low CBF and/or delivery of $^{13}NH_3$ in plasma via collaterals or partially occluded vessels which exclude microspheres. In the latter cases, $^{13}NH_3$ may be more representative of nutrient flow than microspheres. This is particularly evident in regions that had positive ^{13}N concentrations and zero values for microspheres.

Since CBF increases at a faster rate than E decreases, the net extraction (i.e. E times CBF) or tissue ^{13}N concentration (Fig 5 & Table 1) increases monotonically, though nonlinearly, with CBF.

pH, Ammonia Concentration and Metabolism

Phelps et al (30) found no change in E when the pH of the circulating blood was varied from 7.2 to 7.7. This disagrees with results of Carter et al (4) in dogs and Lockwood et al (19) in rats. Carter et al (4) did not control respiration or P_aCO_2 and consequently CBF was allowed to vary. Since the average P_aCO_2 at

the elevated pH was 8 torr higher than at the low pH, the resulting CBF increase of about 11 cc/min/100 gm (25) could have caused the small reported increase in uptake of ^{13}N with increased pH. In addition, the data of Carter et al (4) is not very specific to the brain since the whole head was viewed by the detector and the dog has a small ratio of intra- to extracerebral tissue. Lockwood et al (19) using the Oldendorf technique (23) in rats reported that E for $^{13}NH_3$ significantly decreased as the pH of the injected solution (5% equilibrated Ringer-Hepes buffer, 30 mM, 0.2 mM ammonium acetate and ^3H_2O) was decreased from 8.0 to 6.5. Since the brain is suddenly exposed to anoxia, changes in osmolarity and pressure and CBF was not measured in these experiments, it is difficult to determine the quantitative significance of these results.

One effect of changing the vascular pH is to change the ratio of $^{13}NH_3$ to $^{13}NH_4^+$. Where the steady state distribution of total ammonia (NH_3 and NH_4^+) through the different compartments of the brain will clearly be altered by pH, it is not obvious how a change in the ratio of plasma $^{13}NH_3$ to $^{13}NH_4^+$ will affect the unidirectional transport. The $^{13}NH_4^+$ is expected to have an extremely low extraction (i.e. similar to Na^+ and K^+ which has zero or near zero single pass extraction (17,36)) and $^{13}NH_3$ should be the form extracted to yield large values of E. As $^{13}NH_3$ leaves the vascular compartment it is immediately replaced by the interconversion of $^{13}NH_4^+$ to $^{13}NH_3$. This process is so rapid that it is difficult to see how it could be rate limiting. However, there may be some pH effects that we do not appreciate and that were not large enough to be observed in the pH range of 7.2 to 7.7 reported by Phelps et al (30). In any case, extreme changes in pH are limited in vivo due to hemolysis (30,25).

Phelps et al (30) and Cooper et al (5) found that E was not affected by 17 and 1000 fold increases in blood ammonia levels, indicating that it is unlikely that ammonia diffusion occurs by a saturable carrier. Phelps et al (30) found E reduced

by 24% when glucose and oxygen cerebral metabolism was decreased by a factor of 2.2 in hypoglycemic coma in monkeys. However, in hypoglycemia with elevated ammonia the value of E was unchanged even though oxygen metabolism remained low and glucose metabolism doubled. These data indicate a sensitivity of E to metabolic rate in brain. The hypoglycemia - hyperammonia data are indicative of a detoxification shunt for ammonia (30). Cooper et al (5) found that when methionine sulfoximine (MSO) produced an 86% deactivation of glutamine synthetase in rat brain, that ^{13}N was still rapidly incorporated into glutamine. However, significant changes in the distribution of labeled amino acids occurred; free $^{13}NH_3$ increased and net extraction of $^{13}NH_3$ by brain decreased (the actual amount extracted may not have been reduced since the reduction could have occured only in the amount trapped due to deactivation of glutamine synthatase). These data are for prolonged infusions. The single pass bolus technique would clearly delineate the effects of MSO at the point of forward and back diffusion and metabolic trapping. However, these experiments have not been performed.

The above data, imply that severe reductions in the metabolic trapping mechanism for NH_3 may be required before E is significatly reduced. However, the interpretation of data at the very low values of CBF where reductions in metabolism may also be occuring (i.e. gray, white, mixed values below about 40, 10 and 20cc/min/100gms, respectively) must be done with caution.

Unidirectional Transport/Trapping Model

The Renkin/Crone Model (35,23) is considered to give good estimates of the PS product for stationary CBF states but does not describe the variation of E for $^{13}NH_3$ versus CBF. It is also of limited validity to apply this model to heterogeneous tissue with wide ranges of PS and/or CBF. It has been shown (35) that the total PS determined with this model underestimates the sum of PS values in heterogenous tissue. The "effective" PS values for whole brain and mixed

tissues, shown in figure 8 and Table 1, therefore, underestimate the true values. Basal (i.e. CBF = 40cc/min/100gm) PS values of 22.5 for single pass data and, 21.9 and 23.2 for in vitro mixed tissues agree with the previous estimate of 24cc/min/100gm from Phelps et al (5) in monkey. Tissue sampling experiments to separate gray and white matter (Fig. 5) were performed to resolve the discrepancies of heterogenous tissue. The data demonstrate the differences in net extraction (E times CBF) vs. CBF of relatively pure tissue to that of mixed tissue (Fig. 5).

The estimated PS values from this work (Fig 4, 8, Table 1) indicate that PS does increase with CBF, inferring that capillaries are not rigid Renkin/Crone tubes but increase in surface area and/or permeability with increasing CBF. Since we found no direct evidence in the literature for a mechanism by which capillaries accomodate changes in flow, we used our data to infer a mechanism.

The model description that best fit the data is a "Saturable Recruitment" (SR) Model. In this model all capillaries in the brain are assumed to be identical. At very low CBF few capillaries are open. Increases in CBF occur through recruitment of additional capillaries and increases in the velocity of blood flowing through open capillaries (ie. changes in capillary perfusion pressure). When 100% recruitment of capillaries has occured, further increases in CBF are accomplished by increases in blood velocity. According to the functional form (eq 5) of the SR model $PS = A+B(1-e^{-CF})$, PS is equal to A at zero flow and as flow increases PS increases to a maximum of A + B (i.e. A+B is equal to the PS of all the anatomical capillaries). The rate of increase and the flow value at which the maximum PS is approached is determined by the value of C.

The SR Model allows the capillary PS product to increase with CBF (Fig 8) by an increase in S through recruitment. The model gives a good fit to the E vs CBF and E times CBF vs CBF data in figures 3-5. The white and gray matter data

in figures 5 and 7 illustrate that net extraction of $^{13}NH_3$ at low CBF are similar. However, as CBF increases and white matter capillaries are almost completely recruited, the response of the net extraction of $^{13}NH_3$ (Fig 7) and PS (Fig 8) flattens. On the other hand, gray matter's higher capillary density or greater flow reserve (18) allows further net extraction of $^{13}NH_3$ (Fig. 7) and increases in PS (Fig. 8) at the high values of CBF. At saturation, the ratio of PS values (i.e. A + B in Table 1) for gray to white matter is 60.3/30.6 = 1.97 which should be equal to the anatomical ratio of capillary densities of gray to white matter. In man, the anatomical gray/white capillary density ratio has been reported (18) to be about 3, considerably higher than our value of 2. However, the 10 min half life of ^{13}N limited our ability to completely separate gray and white matter structures. Since the gray/white matter CBF ratio in our experiments was 2.2 and close to the PS saturation ratio of 2, we conclude that the SR model predicts saturation values in good agreement with anatomical capillary ratios of these tissues. The ratio of the rates of PS increase of gray to white matter (i.e. C in Eq. 5 and Table 1) is also 2.

Increases in PS with CBF were also observed in the unidirectional transport and extraction fraction measurements of Bolwig et al (3) for ^{24}Na, ^{14}C-urea, ^{35}S-thiourea and ^{14}C-glucose in the brain of man. These authors report that PS for ^{14}C-glucose increased by 56 and 90% when CBF was increased by 100 and 200% by induced siezure and hypercapnia. Similar trends for ^{24}Na, ^{14}C-urea and ^{35}S-thiourea (even larger increases in PS) were observed (3) but their lower values of E may have limited the accuracy of the PS estimates. Exact values of CBF were not given so an accurate relationship of E vs CBF is not known. These investigators state that their data indicate that some capillaries might be unperfused at normal flows and open up to accomodate increases in flow (3). Pollay and Stevens (31) using rats measured the single pass unidirectional

extraction of ^{14}C-glucose by the brain as a function of CBF in mixed gray and white samples. Using their data we estimated values of effective PS at discrete values of CBF with the Renkin/Crone and the SR model. These data, although statistically limited, indicate that PS for glucose increases by 42% from a CBF of 60 to 120cc/min. At higher CBF, the value of PS did not seem to change. We also used the unidirectional transport data for ^{14}C-glucose of Betz et al (2) in the isolated dog brain to estimate PS as a function of CBF. These data exhibited less statistical scatter than that of Pollay and Stevens and also showed increasing PS with CBF. The shape of the PS vs CBF curve was similar to ours in Figure 8 (i.e. gradual increase to a plateau). The data of Betz et al (2) yielded a 52% increase in PS from a CBF of 20 to 40 cc/min/100gm and a 34% increase from CBF of 40 to 80 cc/min/100gm. All of the above data are in reasonably good agreement with our $^{13}NH_3$ data that also indicate that PS changes by about 40% when CBF is doubled or halved from the basal flow.

The above studies and our data indicate that the PS for a number of substances increases as CBF increases, and that it reaches a constant value at high flows. Since this trend occurs for substances that cross the BBB by either passive or facilitated diffusion, it may be the result of changes in capillary surface area rather than permeability as is indicated in our SR model.

Several investigators have reported similar in PS with blood flow in heart and skeletal muscle that are similar to our results in the brain with $^{13}NH_3$. Yipintsoi et al (43) found a near linear increase in PS for ^{42}K, ^{14}C-glucose and ^{14}C-sucrose over a myocardial flow range in the dog of about 40 to 150 cc/min/100gms. Crone (6) and Renkin (35) found similar results in skeletal muscle. Yudilevich (43) found that the PS product for sucrose in the heart increased with blood flow until at higher flow it became relatively constant and the PS for ^{36}Cl continually increased and did not plateau in the flow range studied

(maximum myocardial flow of only 80cc/min/100gms).

Eichling et al (7) and Raichle et al (32) measured the global single pass extraction of $H_2{}^{15}O$ and labeled alcohols by the brain as a function of CBF in rhesus monkeys. They did not detect increases in PS (analyzed with the Renkin/Crone model) with increasing CBF. However, increases in PS might have been missed because i) the increase with CBF is small (Fig. 8), ii) the near flow limited nature of $H_2{}^{15}O$ and these labeled alcohols make the measurements less sensitive to PS and iii) the small flow range (less than or equal to 30 to 100cc/min/100gms) reduces the detectability of a non linear relationship between ln(1-E) and 1/CBF (i.e. see Fig. 3).

The SR model is a possible explanation of the observations of the relationship between $^{13}NH_3$ extraction, PS and CBF. As to whether the concept of saturable-recruitment is a viable mechanism for changes in capillary flow in the brain requires additional investigative work. Our investigative approach is limited because the results are average values that do not allow inspection or determination of a number of specific variables for the prediction of a detailed mechanism. For example, our method can not directly measure and the model ignores variable capillary lengths and diameters, topology of the vascular bed, up stream and down stream pressures, variable velocity, mechanical properties of blood and vessels, pulsatile flow, and other factors.

Tissue ^{13}N Concentration as an Indicator of Local CBF

Phelps et al (26,30) proposed that $^{13}NH_3$ uptake in brain and heart from i.v. injections could be understood in terms of a unidirectional transport and trapping model and in this respect $^{13}NH_3$ was considered to be analogous to microspheres for capillary blood flow measurements. $^{13}NH_3$ is however, not strictly flow limited in brain and heart and its distribution is dependent upon blood flow, PS, and integrity of the glutamine metabolic trapping mechanism. Recent work of

Norenberg and Martinez-Hernandez (22) demonstrates that glutamine synthetase, exists in equal concentrations in both gray and white matter astrocytes with highest concentrations in the astrocytic pericapillary end-feet in direct contact with capillaries. Thus the principle components of the trapping mechanism have the same distribution as the cerebral capillaries.

While the ^{13}N tissue concentration increases monotonically with CBF, (Fig. 5) the response is nonlinear and the rate of increase diminishes at higher CBF. Doubling or halving CBF from the basal state produces about a 35 to 50% change, depending on the specific tissue and CBF values but further increases produce smaller changes (Fig 7, Table 1). This is a result of ammonia's moderate BBB permeability. Its better flow response in heart is probably due to a factor of four higher capillary density and PS product (37) in the heart. Flow tracers, which are not flow limited, and depend upon a trapping mechanism, are also dependent on both the flow and the rate limiting transport and/or trapping mechanism. Figure 10 shows the calculated response of hypothetical tracers with different PS values assuming a Renkin/Crone capillary model. As PS increases, the response is higher (i.e. the more flow limited the tracer, the more linear the response). While the Renkin/Crone model does not quantitatively predict the flow response, it can be used to qualitatively evaluate potential flow tracers. For example, to determine how high the PS of the tracer must be to yield an acceptable flow response.

The low PS of $^{13}NH_3$ in brain and the normal range of CBF are such that $^{13}NH_3$ is adequate to measure flow reductions but is of limited value at higher values of CBF (Fig. 5).

Increases in BBB permeability accompanying disease may also produce anomalous ^{13}N tissue concentrations. However,some indirect evidence suggests that this may not be as bad as one would initially think. Kuhl et al (15) and Phelps et al (27) have reported positron tomography studies in patients with demonstrated

BBB abnormalities in which regions of maximum $^{13}NH_3$ uptake are adjacent to, but not in regions of maximum BBB damage.

The tissue uptake or CBF reponse has been shown by Phelps et al (30) and Cooper et al (5) to be independent of circulating ammonia concentrations over a 17 and 1000 fold range, respectively. As discussed previously (25) and above, the sensitivity to changes in pH within normal limits appears to be modest or zero.

If the metabolic trapping mechanism is disrupted, the ^{13}N tissue concentration may underestimate CBF. However, large reductions in glutamate/glutamine synthetase activity may be required before any sizable effect is observed in the trapping of tracer quantities of $^{13}NH_3$. Kuhl et al (15) using PCT have studied patients with cerebral ischemia in which regions of decreased glucose metabolism was associated with focal increased $^{13}NH_3$ uptake. In all cases, this apparent "luxury perfusion" state was corroborated by Tc-99m pertechnetate flow studies.

If the substructures of the brain each had different PS products for the same CBF, then each of these substructures would have a different response of $^{13}NH_3$ with changes in CBF. This is seen in the responses of gray and white matter tissues. The capillary density of gray matter is 3 to 4 times white matter (18) and it is seen at high CBF that the gray and white matter responses are significantly different (Fig. 7). This probably occurs among the substructures of gray and white matter but the magnitude is not known.

The trapping mechanism of $^{13}NH_3$ provides a stationary distribution of CBF which is preferred for high quality tomographic imaging (Fig. 1). The procedure is simple and safe, requiring an i.v. bolus injection of $^{13}NH_3$, waiting 3 minutes and imaging.

Measurement of absolute CBF requires measurement of the arterial $^{13}NH_3$ input function (C_b in eq 1) and a calibration factor from figure 5. This was tested

on a preliminary basis using the ECAT and a rhesus monkey, giving a global CBF at a P_aCO_2 of 39mm of Hg of 45 cc/mm/100gms at a P_aCO_2 of 39 mm Hg which is in good agreement with reported basal CBF in monkeys (7). Arterial $^{13}NH_3$ concentration could possibly be approximated by a blood sample from an "arterialized" vein from a heated hand (29). This experiment indicates only the possibility of this approach, more work is required to document its value.

Traditional methods of measuring CBF with external detection of tracers require high temporal resolution to adequately define the tracer washout curve (9,45). Since high count densities are required to provide adequate tomographic images, tomographic washout measurements of CBF will suffer from either poor spatial resolution or poor temporal resolution. Although $^{13}NH_3$ has limitations as an indicator of CBF, all other known flow tracers are also limited and their application in pathology usually amplifies their weaknesses.

TABLE 1: Estimated Values for variables of saturable-recruitment model, $E = (1 - e^{-PS/F})$ where $PS = A + B(1 - e^{-CF})$

Tissue	CBF Range (cc/min/100gm)	A (cc/min/100gm)	B (cc/min/100gm)	C $(cc/min/100gm)^{-1}$	Basal PS* (cc/min/100gm)	A+B+ (cc/min/100gm)
Gray Matter	0-250	10.4 ± 2.9	49.9 ± 3.2	0.0096 ± 0.0021	32.2(F=60)	60.3 ± 4.3
Mixed Gray/ White Matter	0.1-160	7.0 ± 1.8	39.6 ± 3.2	0.0118 ± 0.0027	21.9(F=40)	46.6 ± 3.7
White Matter	0-130	6.2 ± 2.4	24.4 ± 1.9	0.0192 ± 0.0050	14.0(F=20)	30.6 ± 3.1
Cerebellum	8-170	5.8 ± 2.7	52.3 ± 3.9	0.0115 ± 0.0028	31.4(F=60)	58.1 ± 4.7
Compression (Mixed Gray/ White Matter)	1-135	11.8 ± 1.9	27.0 ± 2.7	0.0137 ± 0.0043	23.2(F=40)	38.8 ± 3.3
Single Pass (Mixed Gray/ White Matter)	12-140	9.4 ± 4.5	34.6 ± 5.4	0.0119 ± 0.0065	22.5(F=40)	44.0 ± 7.0

± values are standard errors from least squares fit of data to eq. 5.

* Estimates of basal PS values assuming basal blood flow, F, for gray matter and cerebellum of 60cc/min/100gm. white matter of 20cc/min/100gm and mixed gray/white matter of 40cc/min/100gm.

+ A+B is equal to the total PS of all anatomical capillaries in a given type of tissue.

REFERENCES

1. Berl, S., Takagaki,G., Clarke, D.E., et al: Ammonia and glutamic acid metabolism in brain and liver. J. Biol. Chem. 237:2562-2569, 1962.

2. Betz, A.L., Gilboe, D.D., Yudilevich, D.L. et al: Kinetics and unidirectional glucose transport into isolated dog brain. Am. J. Physiol. 225:586-592, 1973.

3. Bolwig, T.G., Hertz, M.M., Paulson, O.B., et al: Blood brain barrier permeability during hyperosmolarity and during electrically induced seizures in man. In Blood Flow and Metabolism in Brain, Harper, A.M., Jennett, W.B., Miller, J.D., Rowan, J.O. New York, Churchill Livingston, pp 3.3-3.7, 1975.

4. Carter, C.C., Lifton, J.F., Welch, M.J.: Organ uptake and blood pH and concentration effets of ammonia in dogs determined with ammonia labeled with 10 minute-half lived nitrogen-13. Neurology 23:204-213, 1973.

5. Cooper, A.J.L., McDonald J.M., Gelbard, A.S., et al: The metabolic fate of ^{13}N labeled ammonia in rat brain. J. Biol. Chem. 254:4982-4992, 1979.

6. Crone, C.: Permeability of capillaries in various organs as determined by use of the indicator diffusion method. Acta Physiol. Scan. 58:292-305, 1963.

7. Eichling, J.O., Raichle, M.E., Grubb, R.L., Jr., et al: Evidence of the limitations of water as a freely diffusable tracer in brain in the rhesus monkey. Circ. Res. 35:358-364, 1974.

8. Harper, P.V., Lathrop, K.A., Krizek, H., et al: Clinical feasibility of myocardial imaging with $^{13}NH_3$. J. Nucl. Med. 13:278-280, 1972.

9. Holdt-Rasmussen, K.: Regional cerebral blood flow. Acta Neurol. Scand. 43 (Suppl 27):1-81, 1967.

10. Huang, S.C., Phelps, M.E., Hoffman, E.J., et al: Non-Invasive Determination of Local Cerebral Metabolic Rate of Glucose in Man with ^{18}F-Fluoro-2-Deoxyglucose and Emission Computed Tomography: Theory and Results, Am. J. Physiol. (In Press).

11. Hunter, W., Monahan, W.G.: ^{13}N-ammonia: A new physiologic radiotracer for Nuclear Medicine. J. Nucl. Med. 12:368, 1971.

12. Huzman, M.A., Pyane, B.D., Hoffman, J.I.E., et al: Blood flow measurements with radionuclide-labeled particles. Prog. Cardiovasc. Dis. 20:55-79, 1977.

13. Kety, S.S.: The theory and application of the exchange of inert gas at lung and tissues. Parmacol Rev. 3:1-41, 1951.

14. Kuhl, D.E., Phelps, M.E., Hoffman, E.J. et al: Initial clinical experience with ^{18}F-2-Deoxy-D-Glucose for determination of local cerebral glucose utilization by emission computed tomography. IN: Cerebral Function, Metabolism and Circulation. Ingvar, D.G., Lassen, N.A. (Eds). Munksgaard, Copenhagen, pp 192-193, 1977. 56, Munksgaard, Copenhagen, pp 1780179, 1977.

15. Kuhl, D.E., Phelps, M.E., Kowell, A.P., et al: Patterns of local gluocse utilization and perfusion in normal and ischemic brain. Determination in man by emission computed tomography of F-18 fluorodeoxyglucose and N-13 ammonia. Ann. Neurol. (In press).

16. Landau, W.M., Freygang, W.H., Rowland, L.P. et al: The local circulation of the living brain; values in the unanesthetized and anesthetized cat. Trans Am. Neurol. Assoc. 80:125-129, 1955.

17. Lassen, N.A., Trap-Jensen, J., Alexander, S.C., et al: Blood-brain barrier studies in man using the double-indicator method. Am. J. Physiol. 220:1627-1633, 1971.

18. Lierse, W., Horstman, E.: Quantitative anatomy of the cerebral vascular bed with special emphasis on homogeneity and inhomogeneity in small parts of the gray and white matter. In Regional Cerebral Blood Flow, Ingvar, D.G., Lassen, N.A. (eds) Copenhagen, Munksgaard, pp 15-19, 1965.

19. Lockwood, A.H., Finn, R.D., Campbell, J.A. et al: Factors that effect the uptake of ^{13}N ammonia by the brain. J. Comput. Tomo. 2:654-655, 1978.

20. McIlwain, H., Bachelard, H.S.: Biochemistry of the central nervous system. 4th edition, The Williams and Wilkins Co. Baltimore, pp 559, 1966.

21. Monohan, W.G., Tilbury, R.S., Laughlin, J.S.: Uptake of ^{13}N-labeled ammonia. J. Nucl. Med. 13:274-277, 1972.

22. Norenberg, M.D., Martinez-Hernandez, A.: Fine structural localization of glutamine synthetase in astrocytes of rat brain. Brain res. 151:303-310, 1979.

23. Oldendorf, W.H.: Measurement of brain uptake of radiolabeled sustances using tritiated water internal standard. Brain Res. 24:372-376, 1970.

24. Pappenheimer, J.R.: Passage of molecules through capillary walls. Physiol. Rev. 33:387-423, 1953.

25. Phelps, M.E.: Cerebral ammonia metabolism. Stroke 9:521-523, 1978.

26. Phelps, M.E., Hoffman, E.J., Coleman, R.E., et al: Tomographic images of blood pool and perfusion in brain and heart. J. Nucl. Med. 17:603-612, 1976.

27. Phelps, M.E., Hoffman, E.J., Huang, S.C., et al: Design considerations and performance characteristics of the ECAT positron tomograph. J. Comput. Asst. Tomogr. 2:648, 1978.

28. Phelps, M.E., Hoffman, E.J., Huang, S.C. et al: ECAT: A New Computerized tomographic Imaging System for Positron-Emitting Radiopharmaceuticals. J. Nucl. Med. 19:635-647.

29. Phelps, M.E., Huang, S.C., Hoffman, E.J., et al: Tomographic Measurement of Local Cerebral Glucose Metabolic Rate in Man with ^{18}F Fluorodeoxyglucose: Validation of Method, Ann. Nuerol. (In Press).

30. Phelps, M.E., Hoffman, E.J., Raybaud, C.: Factors which effect cerebral uptake and retention of $^{13}NH_3$. Stroke 8:694-702, 1977.

31. Pollay, M., Steven, A.: Simultaneous measurements of regional blood flow and glucose extraction in rat brain. Neurochem. Res. 4:109-123, 1979.

32. Raichle, M.E., Eichling, J.O., Straatmann, M.G., et al: Blood brain barrier permeability of ^{11}C-labeled alcohols and ^{15}O-labeled water. Am. J. Physiol. 230:543-552, 1976.

33. Reivich, M., Kuhl, D.E., Wolf, A., et al: The ^{18}F fluorodeoxyglucose method for the measurement of local cerebral gluocse utilization in man. Circ. Res. 44:127-137, 1979.

34. Renkin, E.M.: Transport of potassium-42 from blood to tissue in isolated manmalian skeletal muscles. Am. J. Physiol. 197:1205-1210, 1959.

35. Renkin, E.M.: Transcapillary exchange in relation to capillary circulation. J. Gen. Physiol. 52:96-108, 1968.

36. Saperstein, L.A.: Regional blood flow by fraction distribution of indicators. Am. J. Physiol. 193:161-168, 1958.

37. Schelbert, H.R., Phelps, M.E., Hoffman, E.J., et al: Regional myocardial perfusion assessed by N-13 labeled ammonia and postiron emission computerized axial tomography. Am. J. Card. 43:208-218, 1979.

38. Sokoloff, L.: Local cerebral circulation at rest and during altered cerebral activity induced by anesthesia on visual stimulation. In: Regional Neurochemistry, Kety, S.S., and Elkes, J. (eds). New York: Pergamon, 1961.

39. Shulman, K., Fusman, M., Rosende, R.: Regional cerebral blood flow. Evaluation of the microsphere technique. In: Cerebral circulation and metabolism. Langfitt, T.W., McHenry, L.C.J., Reivich, M., Wottman, H. (eds). New York, Springer-Verlag, pp 148-151, 1975.

40. Vaalburg, W., Kamphuis, J.A.A., Beerlin-Von der Molen, H.B., et al: An imporved method for the cyclotron production of ^{13}N-labeled ammonia. Int. J. Appl. Rad. Isot. 26:316-318, 1975.

41. Veall, N., Mallett, B.L.: Partition of trace amounts of Xe or between human blood and brain tissues at 37°C. Phys. Med. Biol. 10:375-380, 1965.

42. Warren, S.: Ammonia toxicity and pH. Nature 195:47-49, 1962.

43. Yipintsoi, T., Tancredi, R., Richmon, D., et al: Myocardial extraction of sucrose, glucose and potassium. In: Capillary Permeabiltiy. Crone, C., Lassen, N.A. (eds). New York, Academic Press Inc., pp 153-156, 1970.

44. Yudilevich, D.L.: Serial barrier to blood-tissue transport studied by the single injection indicator diffusion technique. In: Capillary Permeability. Crone, C., Lassen, N.A. (eds). New York, Academic Press, Inc., pp 115-134, 1970.

45. Zieler, K.L.: Equations for measuring blood flow by external monitoring of radioisotopes. Circ. Res. 16:309-321, 1965.

FIGURE CAPTIONS

Figure 1. Comparison of the cross-sectional distribution of the cerebral metabolic rate for glucose measured with FDG and the distribution of intravenously injected $^{13}NH_3$ in two different normal volunteers. Notation of O.M. refers of the cm above the orbital meatus. Brain slices at top are at levels similar to the three right hand FDG and $^{13}NH_3$ images and are shown for anatomical comparison. Note similarity in the distribution of metabolism and $^{13}NH_3$ distribution.

Figure 2. Example of the gray and white matter uptake and clearance of ^{13}N activity subsequent to an intravenous bolus injection of $^{13}NH_3$. $^{13}NH_3$ is rapidly accumulated into the brain due to its relatively free diffussion, rapid clearance from the blood, and its rapid incorporation into glutamine (see Fig 9). From 3 to 50 minutes, there is a very gradual increase in gray and white matter tissue ^{13}N concentration (~15%) due to the very low levels of circulating $^{13}NH_3$ three mins after injection. Subsequent to 60 mins., there is a slow removal of ^{13}N activity from the tissue which probably results from back difussion of free $^{13}NH_3$, ^{13}N-amino acids and from deamination of ^{13}N-amino acids.

Figure 3. Whole brain single pass extraction fraction from intra-carotid bolus injections of $^{13}NH_3$ as a function of CBF in rhesus monkeys. The solid line is a least squares fit to data by eq. 5.

Figure 4. Plot of data from Fig. 3 assuming a Renkin/Crone model as described in eq. 2. A Renkin/Crone model would predict the data to fall on a straight line with a slope of -PS. The data, however, exhibits a nonlinear relationship (i.e. PS changes with CBF) and are best fit by the SR model of eq. 5 that is shown as a solid line.

Figure 5. Plots of net extraction or tissue ^{13}N activity concentrations as a function of CBF. A: net extraction (E x CBF) versus CBF for the whole brain single pass data from rhesus monkeky shown in Fig. 3. B and C: in vitro measured net extraction of $^{13}NH_3$ subsequent to intravenous injection of activity in the dog. Local variations in CBF were produced by a variety of combinations of embolization, respiratory rate, CO_2 gas admixtures and local brain compressions. D: net extraction data when local compressions were produced in either an acute state of compression and release or a chronic state of extended compression and release. E and F: net $^{13}NH_3$ tissue extraction for separated gray and white matter samples as a function of CBF. Variations in CBF were produced by comginations of embolization, local brain compression and P_aCO_2. Solid line is best fit to eq. 5.

Figure 6. Variations in local values of CBF from a basal state to that of a local compression of a section of one hemisphere. The variations in $^{13}NH_3$ tissue concentration follow the variations in flow in both the hemisphere with compression and the contralateral hemisphere, although the increases and decreases in tissue ^{13}N concentration tend to be less than the changes in CBF as would be expected from Fig. 5. All samples contained admixtures of gray and white matter.

Figure 7. Combined plot of equations shown in Table I and Fig. 5. The difference between the equations at CBF values less than about 40 are not statistically significant. Note similarity in response of gray matter with the high capillary density tissue of cerebellum, similarities of the mixed gray and white matter from in vivo single pass and in vitro net extraction data, and the lower response and rapid flattening of the curve for white matter due to its low CBF reserve and capillary density (see Discussion Section on SR model).

Figure 8. Combined plots of PS product as a function of CBF from fits of the data in fig. 5 to the SR model of eq. 5.

Figure 9. Schematic representation of the unidirectional transport of $^{13}NH_3$ from the vascular pool through the blood brain barrier (BBB) and the rapid incorporation into primarily glutamine through the small glutamate - glutamine synthatase pool (5,1) located in the astrocytes (10). Thick arrows indicate the unidirectional nature of the transport and trapping subsequent to either an intra corotid or intravenous bolus injection of $^{13}NH_3$. The ^{13}N glutamine then communicates with a large glutamine pool which exhibits a slow turnover rate, as exemplified by the relatively slow clearance of ^{13}N activity from the brain shown in Fig. 2.

Figure 10. Plot of the flow response (i.e. net tissue extraction or concentration of tracer) for tracers with different PS products using Renkin/Crone Model. Although the rigid tube Renkin/Crone model does not predict the exact flow response, it can be used for guidance in the selection of non-flow limited tracers for their potential use as indicators of blood flow in a unidirectional transport and trapping approach. Although, the highest possible PS product is desirable, it is quite apparent that acceptable flow responses over a given flow range can be achieved with tracers with less than ideal values of PS. However, a lower limit in the value of PS produces unacceptable flow responses. It should be noted that any mechanisms which increases capillary surface area as flow increases (i.e. SR model) will improve the flow response as compared to the rigid tube Renkin/Crone prediction.

ACKNOWLEDGEMENTS

We would like to thank Ms. JoAnne Miller, Ms. Francine Aguilar, for their technical assistance, Mrs. Lee Griswald for the illustration work and Dr. H. Schelbert for his many helpful discussion. Dr. N.S. MacDonald and his cyclotron crew and Gerald Robinson and his chemistry staff's efforts and help are deeply appreciated.

$^{13}NH_3$ is used to represent the chemical equilibrium

$^{13}NH_3 \; H_2O \rightleftharpoons NH_4^+ \; OH^-$

§ 3M Company, Nuclear Products, St. Paul, MINN.

† ORTEC, INC., Oak Ridge, TENN.

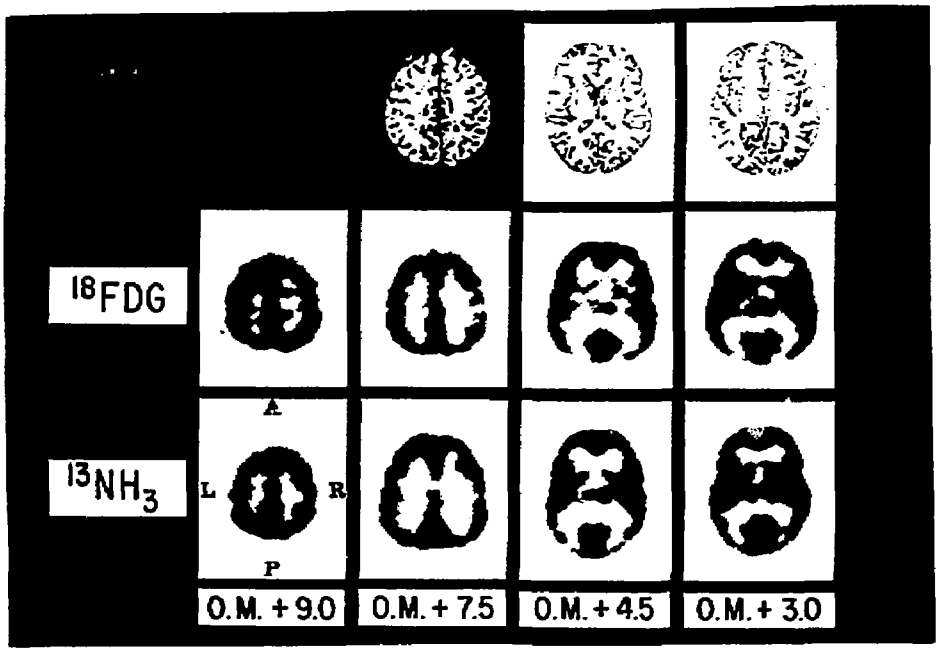
18FDG
13NH3
A
L
R
P
O.M. + 9.0
O.M. + 7.5
O.M. + 4.5
O.M. + 3.0

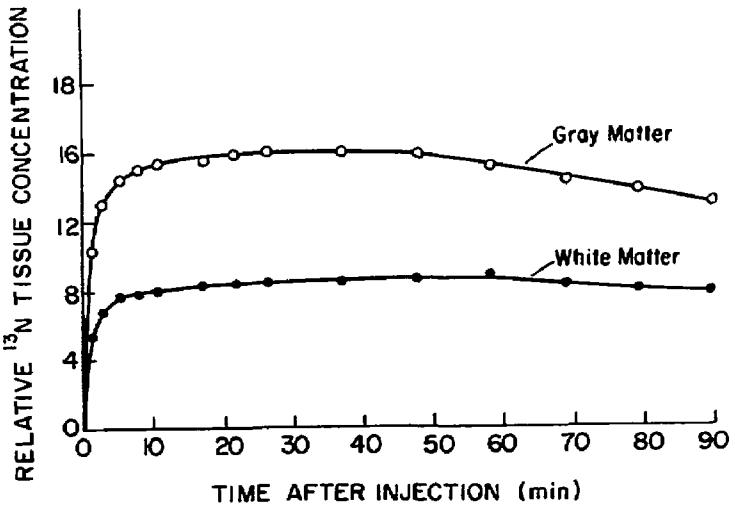
RELATIVE 13N TISSUE CONCENTRATION
0
4
8
12
16
18
0
10
20
30
40
50
60
70
80
90
TIME AFTER INJECTION (min)
Gray Matter
White Matter

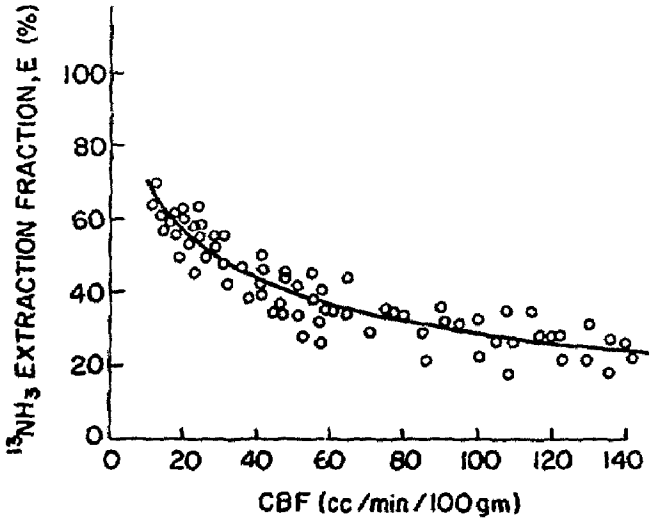
$^{13}NH_3$ EXTRACTION FRACTION, E (%)
100
80
60
40
20
0
0
20
40
60
80
100
120
140
CBF (cc/min/100gm)

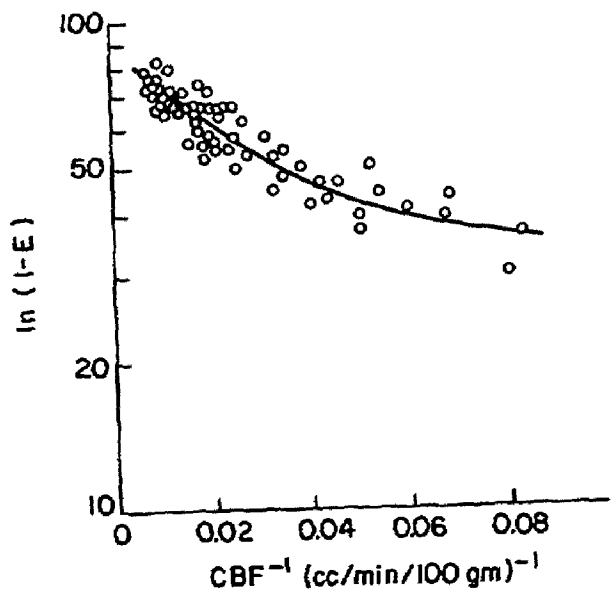
100
50
20
10
ln (1-E)
0
0.02
0.04
0.06
0.08
CBF^{-1} (cc/min/100 gm)$^{-1}$

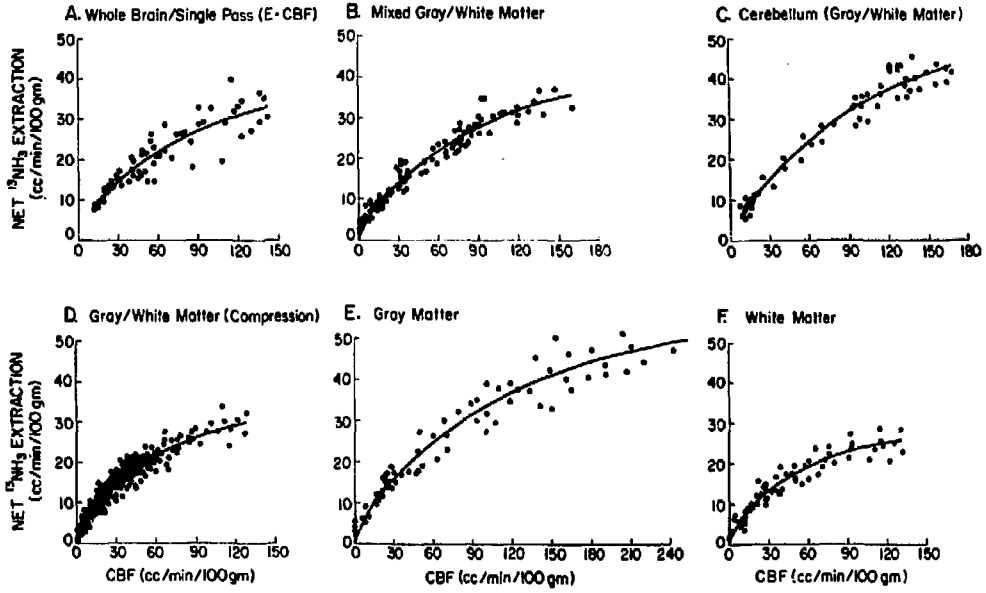
A. Whole Brain/Single Pass (E·CBF)
B. Mixed Gray/White Matter
C. Cerebellum (Gray/White Matter)
D. Gray/White Matter (Compression)
E. Gray Matter
F. White Matter
NET $^{13}NH_3$ EXTRACTION (cc/min/100 gm)
CBF (cc/min/100 gm)

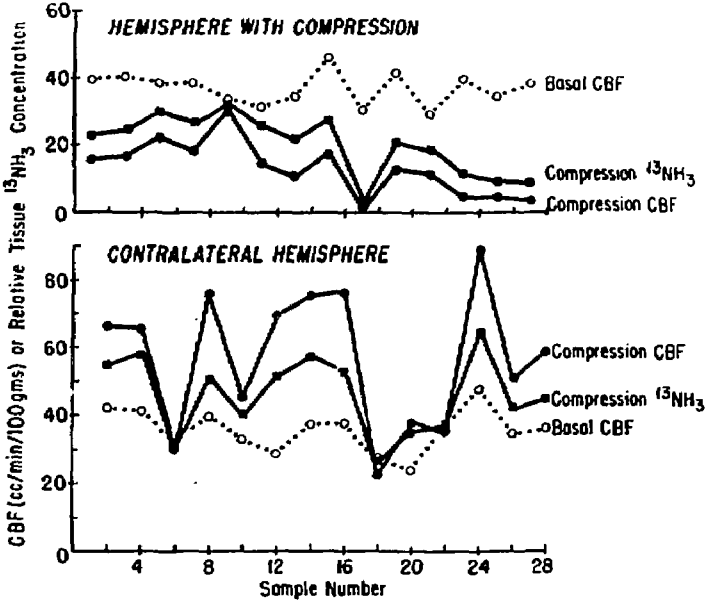
HEMISPHERE WITH COMPRESSION
Basal CBF
Compression $^{13}NH_3$
Compression CBF
CONTRALATERAL HEMISPHERE
Compression CBF
Compression $^{13}NH_3$
Basal CBF
CBF (cc/min/100gms) or Relative Tissue $^{13}NH_3$ Concentration
Sample Number
0
20
40
60
80
4
8
12
16
20
24
28

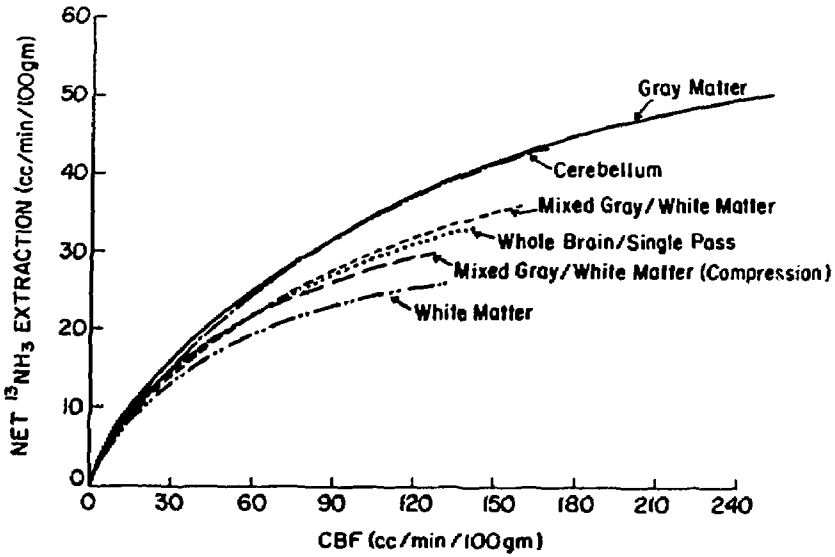
NET $^{13}NH_3$ EXTRACTION (cc/min/100gm)
60
50
40
30
20
10
0
0
30
60
90
120
150
180
210
240
CBF (cc/min/100gm)
Gray Matter
Cerebellum
Mixed Gray/White Matter
Whole Brain/Single Pass
Mixed Gray/White Matter (Compression)
White Matter

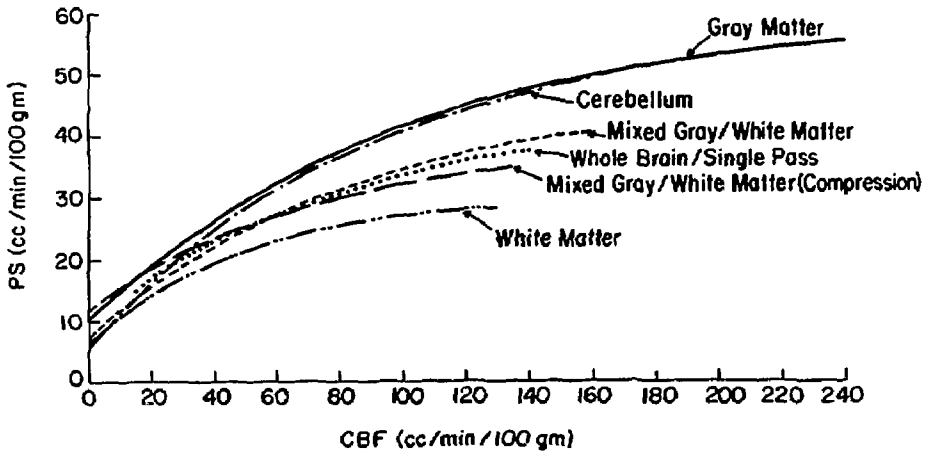
PS (cc/min/100gm)
60
50
40
30
20
10
0
0
20
40
60
80
100
120
140
160
180
200
220
240
CBF (cc/min/100gm)
Gray Matter
Cerebellum
Mixed Gray/White Matter
Whole Brain/Single Pass
Mixed Gray/White Matter(Compression)
White Matter

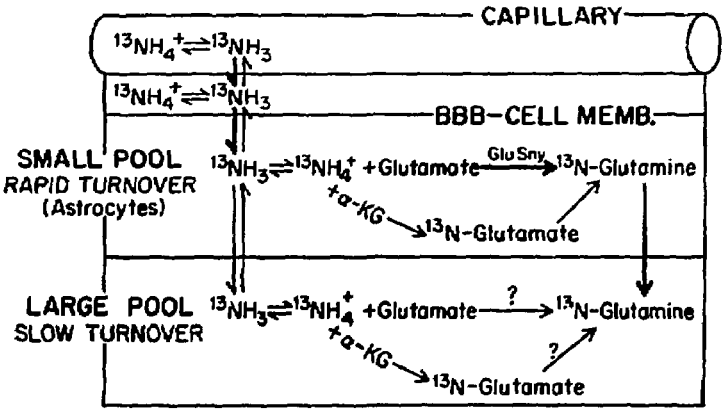
CAPILLARY
$^{13}NH_4^+ \rightleftharpoons {}^{13}NH_3$
$^{13}NH_4^+ \rightleftharpoons {}^{13}NH_3$
BBB–CELL MEMB.
SMALL POOL
RAPID TURNOVER
(Astrocytes)
$^{13}NH_3 \rightleftharpoons {}^{13}NH_4^+$ +Glutamate
Glu Syn
^{13}N-Glutamine
+α-KG
^{13}N-Glutamate
LARGE POOL
SLOW TURNOVER
$^{13}NH_3 \rightleftharpoons {}^{13}NH_4^+$ +Glutamate
?
^{13}N-Glutamine
+α-KG
?
^{13}N-Glutamate

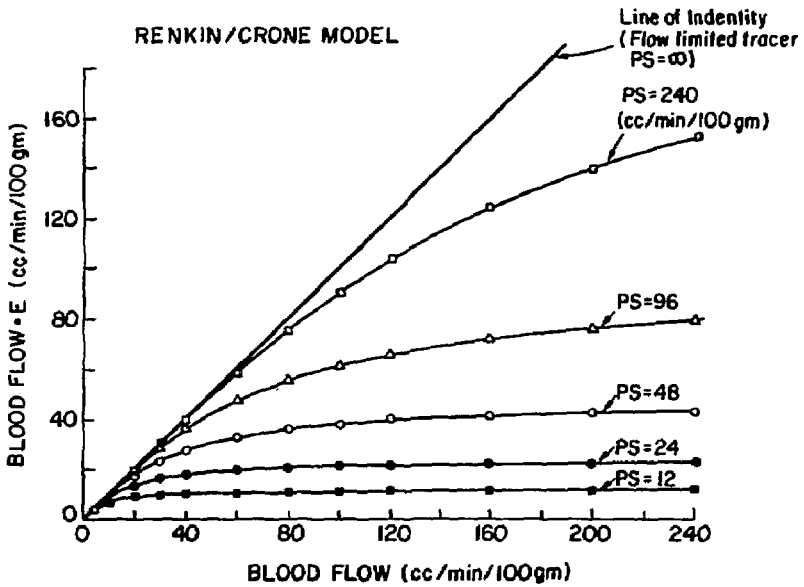
RENKIN/CRONE MODEL
Line of Indentity
(Flow limited tracer
PS=∞)
PS=240
(cc/min/100gm)
PS=96
PS=48
PS=24
PS=12
BLOOD FLOW • E (cc/min/100gm)
0
40
80
120
160
200
240
BLOOD FLOW (cc/min/100gm)